Atomistic studies of temporal characteristics of polarization relaxation in ferroelectrics

Jianyi Liu [1,2,3] Haohua Wen [1,2,3,*] Weijin Chen,[1,2,4] and Yue Zheng[1,2,†]

[1]*Centre for Physical Mechanics and Biophysics, Sun Yat-sen University, Guangzhou, 510275, China*

[2]*State Key Laboratory of Optoelectronic Materials and Technologies, School of Physics, Sun Yat-sen University, Guangzhou 510275, China*

[3]*Sino-French Institute of Nuclear Engineering and Technology, Sun Yat-sen University, Zhuhai 519082, China*

[4]*School of Materials, Sun Yat-sen University, Shenzhen 518107, China*

(Received 9 July 2020; revised 30 October 2020; accepted 3 December 2020; published 19 January 2021)

Polarization relaxation fundamentally determines the speed, energy consumption, and functionality of ferroelectric materials and devices, which is considered as the core aspect of ferroelectric-based applications and attracts considerable attention. The relaxation time, describing the temporal characteristics of polarization relaxation, has been reported to vary from subpicoseconds to hundreds of nanoseconds in ferroelectrics, and the microscopic picture is still an open question. In this paper, starting from atomistic models for ferroelectrics, a generalized Langevin equation is proposed to describe the dynamical behaviors of polarization at the mesoscale or macroscale. On one hand, through the artificial construction of adiabatic processes, it is derived that the relaxation time is connected with the lifetimes of the phonon modes involved in a many-body ferroelectric system, bridging the thermodynamics of polarization with the dissipation behavior of the phonon modes at the microscale. On the other hand, the relaxation time is then linked to the kinetic coefficient used in the time-dependent Ginzburg-Landau equation, for the polarization evolution on the meso- or macroscale. Furthermore, based on driven Brownian motion, we propose a theoretical model of the dependence of the polarization switching time with an applied external electric field on a ferroelectric monodomain system. The prediction of the switching time is found to agree well with the dynamical simulation data, which verifies the applicability and reliability of the physical picture of the relaxation time clarified in the current work. Our discussion of the physical picture of the polarization relaxation time provides useful ideas for the development of multiscale modeling method for ferroelectrics.

DOI: 10.1103/PhysRevB.103.014308

I. INTRODUCTION

The observed polarization of a ferroelectric material is the result of free energy minimization under a specific external environment. With sudden changes in the environment of a ferroelectric material, a dynamic process is present, where the polarization evolves towards a new equilibrium state, which is the so-called polarization relaxation. Polarization relaxation fundamentally determines the speed, energy consumption, and functionality of ferroelectric materials and devices, and is considered the core aspect of ferroelectric-based applications. Much academic attention and continuous research work have been devoted to the responses of ferroelectric polarization under the stimulation of electrical, mechanical, thermal, and optical loading [1–5].

The temporal characteristics of polarization relaxation are usually described by the relaxation time τ of polarization during the dynamic process [6]. For ferroelectric materials, the relaxation time is reported to cover a wide order of magnitude, from subpicoseconds to hundreds of nanoseconds [7–15]. In addition, the estimations of relaxation time obtained with theoretical models and experimental measurements, and even with different theoretical calculations, can differ vastly. The causes of the related issues can generally be attributed to two aspects. On one hand, many possible factors could be responsible for macroscopic polarization, including electric dipoles (called "dipole" in the rest of the paper), domain walls, and space charges, so polarization relaxation is the synergistic effect of the relaxation of dipoles, domain walls, and space charges, which covers a wide range of timescales [16–18]. On the other hand, theoretical models or experimental measurements for studying polarization relaxation rely on different collective representations of macroscopic polarization. For example, the polarization relaxation process is carried out by the dynamics of positive and negative ions in molecular dynamics (MD) simulations [19–23] and by local mode relaxation in the effective Hamiltonian method [24–26]. In addition, the phase field model (PFM) of ferroelectrics describes polarization relaxation by a transport equation, i.e., the time-dependent Ginzburg-Landau (TDGL) equation. The temporal evolution of polarization is fully governed by the kinetic coefficient L, whose value has been of enormous interest [27,28]. In this regard, the prediction of relaxation time relying on different theoretical methods employed [23,26,28] yields confusing discrepancies. To clarify abovementioned inconsistencies, a well-defined theoretical framework bridging models of polarization relaxation on various length scales is required [29–33]. Here, the physical picture of the polarization relaxation time τ

*Corresponding author: wenhh3@mail.sysu.edu.cn

†Corresponding author: zhengy35@mail.sysu.edu.cn

is one of the key issues and is the primary focus of the current paper.

The widely considered polarization switching in ferroelectric materials, a typical kind of relaxation process, is an excellent example for discussing the physical picture of relaxation time. Polarization switching dynamics induced by an applied external field (either electric field or mechanical strain) are implemented by the reversals of microscopic local domains. During this process, microdomains go over an energy barrier F_m [e.g., which is suppressed by applying a reversed external electric field E as shown in Fig. 1(d)] under thermal assistance. In the case of a smaller E, i.e., $E < E_{\text{crit}}$ with E_{crit} being the thermodynamic coercive field [34], where F_m is suppressed mildly while still larger than the thermal energy $k_{\text{B}}T$ (i.e., $F_m(E) > k_{\text{B}}T$), the polarization switching is treated as a quasiequilibrium process, so the characteristic relaxation time τ can be described by the Arrhenius law (or classical nucleation theory) well [34–36], i.e.,

$$\tau^{-1} \propto \omega_A \exp(-F_m(E)/k_{\text{B}}T), \tag{1}$$

where ω_A is the fluctuation frequency near the bottom of the potential well. In fact, most experimental data are obtained under this small field condition $E < E_{\text{crit}}$ [34], and theoretical predictions are usually based on the principle of the Arrhenius law. However, in the case of the application of a high reversed field E (i.e., $E \geqslant E_{\text{crit}}$), where F_m is significantly suppressed and is comparable to or smaller than $k_{\text{B}}T$ (i.e., $F_m \leqslant k_{\text{B}}T$), the polarization switching is then a nonequilibrium process that can be treated as driven Brownian motion inside a stochastic medium. Therefore, τ is determined by the damping constant γ arising from the many-body effects of the thermal fluctuations of ions inside the ferroelectric materials as [37]

$$\tau^{-1} \propto \gamma(E - E_{\text{crit}}). \tag{2}$$

Brownian motion is a quite common mechanism of the phase transport process with low activation energies [38] (i.e., $F_m \leqslant k_{\text{B}}T$), such as kink diffusion along dislocation lines [39], migration of dislocation loop [40], and solute diffusion [41,42]. Some studies [43–46] also report on the issues of homogeneous polarization switching under the application of a large electric field. Interestingly, there are not many studies on ultrafast polarization switching with respect to the driven Brownian motion mechanism under a high field $E \geqslant E_{\text{crit}}$; in particular, microdynamic insight into the damping constant for polarization evolution due to the many-body effects arising from thermal fluctuations of ions inside ferroelectric materials is lacking. Based on the physical picture of polarization relaxation time proposed in the current work, we aim to discuss this interesting issue.

In this paper, we use atomistic simulations based on core-shell interatomic potentials [47] to study the polarization relaxation process in a defect-free $BaTiO_3$ (BTO) ferroelectric monodomain system. This paper is organized as follows: A theoretical model of the temporal characteristics of polarization relaxation is proposed in Sec. II, bridging the microdynamics and thermodynamics. In Sec. III, the temperature dependence of the polarization relaxation time in different ferroelectric phases of BTO is estimated by performing molecular dynamics (MD) simulations of the intrinsic polarization dynamics during artificially designed adiabatic processes. In Sec. IV, we link the relaxation time with the kinetic coefficient used in phenomenological models, e.g., the TDGL equation, governing the meso- or macroscale polarization evolution behavior. Then, following the role of driven Brownian motion, a theoretical model of the polarization switching time under an applied large electric field is derived for comparison with dynamical simulation results, based on which we discuss the applicability and reliability of the physical picture of relaxation time proposed in Sec. II. The conclusion is drawn in Sec. V.

II. THEORETICAL MODEL

For a neutral ferroelectric system including numbers of positive and negative ions, the intrinsic lattice dynamics are governed by a many-body Hamiltonian $\mathcal{H}$

$$\mathcal{H} = \sum_i \frac{\boldsymbol{p}_i^2}{2m_i} + U(\{\boldsymbol{r}_i\}) + \mathcal{H}_{\text{env}}. \tag{3}$$

Here, $\boldsymbol{p}_i$, $\boldsymbol{r}_i$, and m_i are the atomic momentum, coordinates, and mass, respectively. $U(\{\boldsymbol{r}_i\})$ describes the many-body interatomic interactions, and $\mathcal{H}_{\text{env}}$ represents the external actions, such as the thermostat and applied external field. When this ferroelectric system stays in a thermodynamic equilibrium state, the lattice dynamics can be equivalently represented by the thermal distribution of intrinsic phonon modes [48]

$$\mathcal{H} = E_0 + \sum_k n_k \hbar\omega_k + \mathcal{H}', \tag{4}$$

where E_0 is the static state energy at $T = 0$ K, ω_k is the vibrational frequency of the phonon modes $|k\rangle$, n_k is the occupation number, and $\mathcal{H}'$ represents the phonon-phonon interactions. In this case, the phase space associated with the lattice dynamics of the system of interest is constructed by the complete base of the eigenvectors of the phonon modes $\{|k\rangle\}$. According to statistical thermodynamics, the time-dependent polarization $P(t)$ is a thermodynamic observable (or ensemble average) of the polarization operator $\hat{P}(t) = \sum q_i \hat{r}_i(t)$ (q_i is the Born effective charge of the ith ion) over the phase space, as $P(t) = \sum_k \langle k|\hat{P}(t)|k\rangle$.

Following the projection operator approach [49,50], the many-body system $\mathcal{H}$ of Eq. (4) can also be described in space with $|P\rangle$ as the base, which is the eigenvector of $\hat{P}$, and $|P\rangle = \sum_k |k\rangle \langle k|P\rangle$. A generalized Langevin equation (GLE) can then be used to describe the stochastic evolution behavior of the observed polarization $P(t)$, i.e.,

$$m^*\ddot{P} = -\partial_P F(P) - m^*\gamma\dot{P} + f(t), \tag{5}$$

where $F(P)$ is a conserved potential field [51], so the term $-\partial_P F(P) = -\partial F/\partial P$ acts like the conserved generalized force for $P(t)$; $f(t)$ is a Gaussian-type random force field, and $-m^*\gamma\dot{P}$ represents the dissipation, with m^* and γ representing the effective mass and the dissipation coefficient, respectively. Note that the GLE of Eq. (5) can be treated as a coarse-grained equation for polarization evolution, similar to that in recently developed dynamical phase-field model (d-PFM) [28]. As thoroughly addressed in Ref. [51], the action of the thermal motion of ions, i.e., lattice dynamics, is considered coarse grained in the provision of the generalized potential force field for polarization evolution. In addition, Eq. (5) is

reduced to the phenomenological equation of motion by Tani [52] if $f(t) = 0$ and $-\partial_P F = -m^*\chi(\partial F/\partial P)$, and is further reformed to the original transport equation by Landau and Khalatnikov [53] by neglecting the term $m^*\ddot{P}$. In this regard, Eq. (5) is in fact a macro- or mesoscale evolution equation, using a finite number of quantities defined in phase space to represent a large number of microdynamic degrees of freedom involved, so all the terms intrinsically have a many-body nature. Therefore, determining the microdynamic source of the mesoscale parameter γ, as well as others in Eq. (5), can help us to obtain deep insight into the thermodynamics of the ferroelectric phase transition, which is considered a key step in the development of a multiscale modeling scheme in materials science [29].

According to Eq. (5), γ could be measured as the damping constant of polarization during an adiabatic relaxation process. Therefore, we analyze macroscopic polarization relaxation behavior based on Eq. (5) and microscale dynamical behaviors of ions in ferroelectric systems to discuss the physical picture of γ.

An adiabatic process based on Eq. (5) can be designed by detaching the system from its noisy environment by setting $f(t) = 0$ in Eq. (5) and initializing the system at an excited state denoted by P_0 at the moment of $t = 0$ near its equilibrium state P_A, as shown in Fig. 1(d). We assume that $F(P)$ can be expanded harmonically near P_A as

$$F(P) = F(P_A) + m^*\omega_A^2(P - P_A)^2 \tag{6}$$

with ω_A being the characteristic fluctuation frequency. Therefore, the system adiabatically relaxes towards P_A like a damped oscillator over time, and $P(t)$ is determined by

$$m^*\ddot{P} + m^*\gamma\dot{P} + m^*\omega_A^2(P - P_A) = 0. \tag{7}$$

In the case of the underdamped condition, i.e., $\gamma < 2\omega_A$, the time-dependent trajectory of $P(t)$ is given by

$$P(t) = P_A + (P_0 - P_A)e^{-t/2\tau}\cos(\omega' t + \phi), \tag{8}$$

where ϕ is a phase angle, $\tau = \gamma^{-1}$ is the defined polarization relaxation time, ω' is a modified frequency, and $\omega' = \sqrt{\omega_A^2 - \gamma^2/4}$. In particular, $\omega' \approx \omega_A$ in the limit of $\gamma \ll 2\omega_A$, under which the energy reduction rate is thus written as

$$F(t) - F_A = (F_0 - F_A)e^{-t/\tau}, \tag{9}$$

where $F(t) = F(P)$, $F_A = F(P_A)$, and $F_0 = F(P_0)$.

Let us discuss the microdynamics insight into the adiabatic process mentioned above. Before the adiabatic relaxation process, the ensemble of phonon modes $\{|k\rangle\}$ in the ferroelectric system described by Eq. (4) has an equilibrium distribution represented by the occupation number $\{n_k\}$, which is regarded as the phase coordinate in the phonon phase space constructed by $\{|k\rangle\}$. At the moment of $t = 0$, artificially "moving" the polarization P away from its equilibrium state P_A to an excited state P_0 increases the "potential energy" of P by $\Delta F = F_0 - F_A > 0$, which is also equivalent to bringing all the phase space coordinates from $\{n_k^{P_A}\}$ denoted by P_A to $\{n_k^{P_0}\}$ denoted by P_0. In this case, the subsequent adiabatic relaxation process in terms of $P(t)$ from P_0 to P_A is in fact *moving* the many-body system from $\{n_k^{P_0}\}$ towards $\{n_k^{P_A}\}$ due to the phonon-phonon interaction in the phase space constructed by the eigenvectors $\{|k\rangle\}$ of the phonon modes. Note that the time evolution of $n_k(t) = n_k^{P(t)}$ is as follows

$$n_k(t) = n_k^{P_A} + \left(n_k^{P_0} - n_k^{P_A}\right)e^{-t/\tau_k}. \tag{10}$$

Here, $n_k^{P(t)} = \langle P|\hat{n}_k(t)|k\rangle$ denotes the projection of $(\hat{n}_k\,|k\rangle)$ on $|P\rangle$, and τ_k is the lifetime of phonon mode $|k\rangle$.

According to statistical thermodynamics, the total energy of the ensemble of phonon modes is fixed during an adiabatic process; thus, the heat dissipation rate $\dot{Q}$ is equivalent to the reduction rate of free energy $\dot{F}$, which is associated with polarization in the current system shown in Eq. (6) [51]; i.e., $\dot{Q} = -\dot{F}$. In the phonon system, the heat dissipation rate $\dot{Q}$ is determined by the entropy production rate as

$$\dot{Q} = \sum_k T_k\dot{S}_k = \sum_k \dot{n}_k\hbar\omega_k, \tag{11}$$

where T_k and S_k are the temperature and entropy for the specific phonon mode $|k\rangle$; i.e., $T_k = n_k\hbar\omega_k/k_B$ and $S_k = k_B(\ln n_k + 1)$, respectively. Note that the total amount of heat production Q is equal to the free energy reduction $F_0 - F_A$ for the whole adiabatic process from P_0 to P_A; i.e., $Q = F_0 - F_A$. In addition, at any arbitrary moment t during the adiabatic relaxation process, the accumulated heat production $Q(t)$ is equal to the reduction in free energy, i.e., $Q(t) = F_0 - F(t)$, which is then derived as

$$\frac{\int_t^\infty \dot{Q}(t')dt'}{Q} = \frac{F(t) - F_A}{F_0 - F_A} = e^{-t/\tau}. \tag{12}$$

Combining Eqs. (10), (11), and (12), we have

$$e^{-t/\tau} = \langle e^{-t/\tau_k}\rangle \quad \Rightarrow \quad \tau = \langle\tau_k\rangle. \tag{13}$$

Here, the detailed deduction can be seen in Sec. SI of the Supplemental Material [54]. Equation (13) is the bridge connecting the microscale dynamics based on lattice dynamics and the mesoscale or macroscale polarization evolution, where polarization relaxation is implemented through momentum and energy transfer between the phonon modes in a many-body system due to the intrinsic anharmonic effects arising from phonon-phonon collisions. In the following, taking BTO as an example, we perform MD simulations to generate the adiabatic trajectories of polarization and then calculate the intrinsic relaxation time τ following Eq. (8).

III. SIMULATIONS OF THE POLARIZATION RELAXATION TIME

We take BTO as an example to investigate the temporal characteristics of polarization relaxation. BTO is a typical ferroelectric material, presenting a tetragonal (T) phase with spontaneous polarization along the z direction with $P_z = \lambda(\approx 0.2\ \mathrm{C/m^2})$ at room temperature (300 K) [55]. The landscape of the Helmholtz free energy $F(P)$ for a monodomain structure of BTO is calculated beforehand, which helps us to describe the selection of initial states and the design of the adiabatic relaxation process for our later simulations for the evaluation of the polarization relaxation time. In the current paper, the $F(P)$ of BTO (containing $16\times16\times16$ unit cells) at 300 K is calculated using the thermodynamic integration approach in MD simulations under the constraint of fixed po-

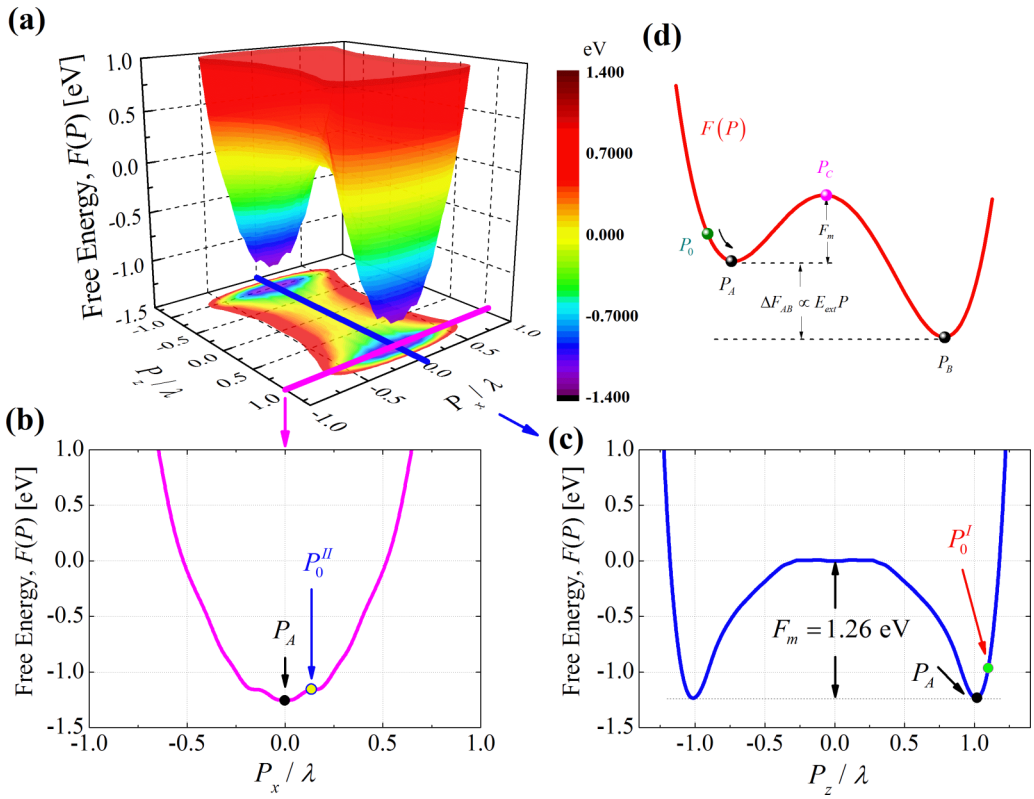

FIG. 1. Free energy of bulk $BaTiO_3$ at room temperature. (a) The free energy landscape $F(P)$ with 16×16×16 unit cells using thermodynamic integration based on the first-principles-derived effective Hamiltonian method [57], as well as the free energy profile along the (b) ⟨100⟩ and (c) ⟨001⟩ directions. Here, $F_m = 1.26$ eV (∼0.3 meV per unit cell [57]) is the migration energy, $P_A = (0, 0, 1)\lambda$ represents the equilibrium state with $\lambda \approx 0.2(\mathrm{C/m^2})$, and P_0 is an excited state near P_A. (d) Schematics of a bias double well model of relaxation in phase space denoted by the polarization P.

larization based on a first-principle-derived effective Hamiltonian for BTO [56–58]. In addition, the free energy landscape calculation is performed with a fixed strain tensor so that only two equivalent minima are expected along the spontaneous polarization direction, e.g., ⟨001⟩ or the z direction, as shown in Fig. 1. Section SII of the Supplemental Material [54] provides more detailed information about the free energy calculation. Figures 1(a), 1(b), and 1(c) plot the free energy landscape of BTO at room temperature on the {010} plane and the projection along the ⟨100⟩ and ⟨001⟩ directions, respectively. It is found that $F(P)$ has a local minimum at $P_x = 0$ along the ⟨100⟩ direction and a typical double well structure along ⟨001⟩ with two minima at $P_z = \pm\lambda$ denoting two symmetrical global equilibrium states, as well as a local maximum $P_z = 0$. Moreover, the energy barrier of the phase transition between these two minima of $P_z = \pm\lambda$ is found to be approximately 1.26 eV (∼0.3 meV per unit cell), which is consistent with other calculation results [57].

To investigate the temporal characteristics of polarization relaxation from a microdynamic point of view through the designed adiabatic processes, MD simulations based on the core-shell model [47] are performed in the current paper, which can correctly reproduce the sequence of the phase transition of BTO (see Fig. S1 in the Supplemental Material [54]). Furthermore, the power spectra of the trajectory $P(t)$ show three response frequency bands located at approximately 8 THz, 70 THz, and 200 THz, corresponding to the responses of the total polarization, dipoles in a unit cell, and core-shell interaction, respectively. A significant difference in the power spectra along the polar and nonpolar directions is found in the lowest frequency band (i.e., ∼8 THz for the total polarization responses), based on which the relaxation time is estimated (see Fig. S2 in the Supplemental Material [54]). Here, the polar and nonpolar directions are defined as the directions with and without spontaneous polarization, respectively, in a specific phase.

In the MD, all the thermodynamic quantities rely on the atomic configuration $\{\boldsymbol{r}_i, \dot{\boldsymbol{r}}_i\}$, including the polarization, temperature, and the initial states we need here. However, the implementation of the initial states by an atomic configuration $\{\boldsymbol{r}_i, \dot{\boldsymbol{r}}_i\}$ in MD simulations is quite a challenging task. First, the initial state P_0 is a state located at the free energy landscape, so the variances of the atomic displacements and momenta based on the atomic configuration $\{\boldsymbol{r}_i, \dot{\boldsymbol{r}}_i\}$ should be set to follow the Maxwell-Boltzmann distribution denoted by the background temperature, e.g., $T = 300$ K. Second, based on the configuration $\{\boldsymbol{r}_i, \dot{\boldsymbol{r}}_i\}$, the calculated total polarization should be equal to the preset polarization, which exhibits a small deviation from its equilibrium value. Considering the numerical implementation, two typical kinds of initial states in the T phase of BTO are adopted for the adiabatic processes in our simulations, as shown in Fig. 1, i.e., Case I with $P_0^I = (0, 0, 1 + \Delta)\lambda$ and Case II with $P_0^{II} = (\Delta, 0, 1 + \Delta)\lambda$, with $P_A = (0, 0, 1)\lambda$ and $\Delta \ll 1$ denoting a small deviation.

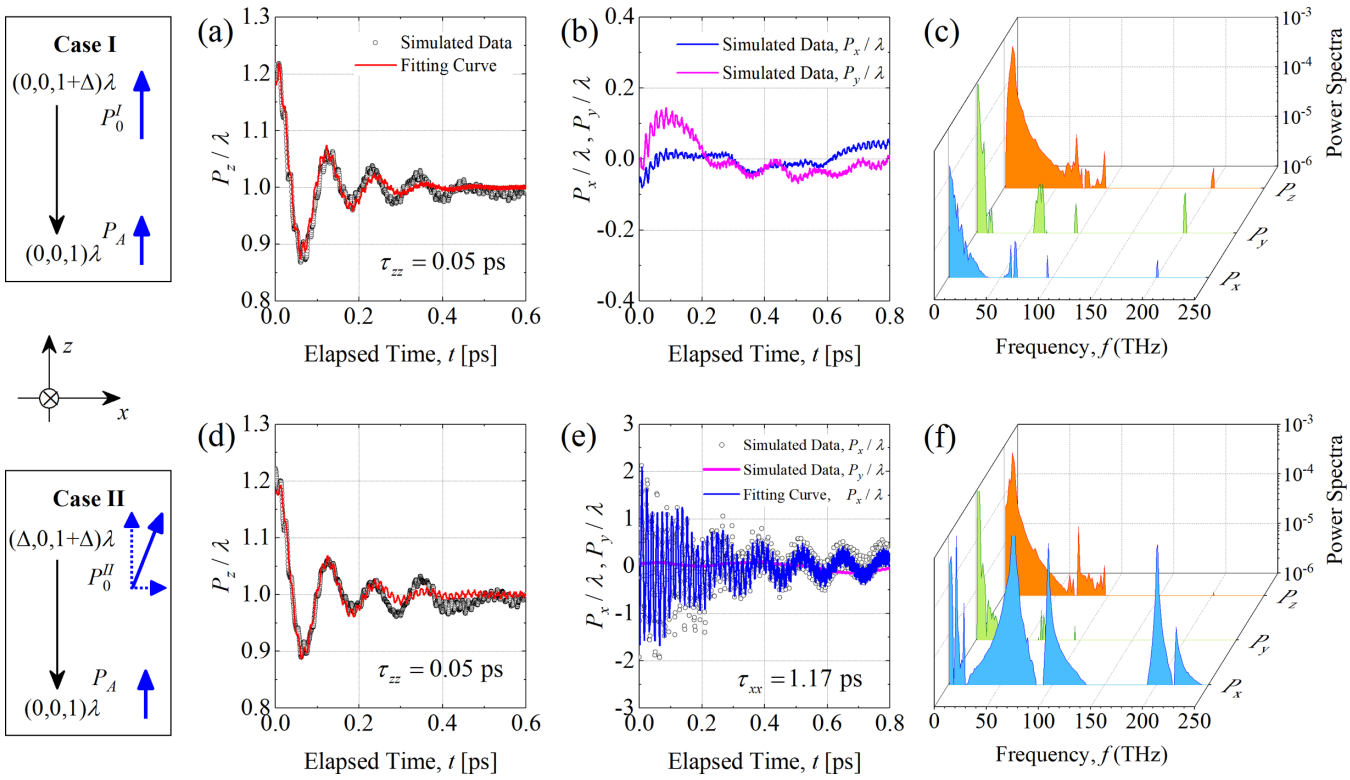

FIG. 2. The relaxation processes of polarization in $BaTiO_3$ at 300 K. The time dependence of the observed (a) $P_z(t)$ and (b) $P_x(t)$ and $P_y(t)$ and (c) the corresponding power spectra in Case I. (d), (e), and (f) show the same relaxation details for Case II.

Here, Case I is used to investigate the relaxation behavior along the polar direction, and Case II is used to investigate the relaxation behaviors along the nonpolar directions, as well as the coupling between the polar and nonpolar directions. Readers can refer to Sec. SIV in the Supplemental Material [54] to obtain more detailed information.

In the MD simulations for an adiabatic process, the simulation box of BTO is set to be $12\times12\times12$ unit cells containing 8640 atoms. The many-body system is first initialized in an excited state denoted by P_0 (slightly deviating from the equilibrium state denoted by P_A, as shown in the schematic in Fig. 1) by giving an atomic configuration $\{\boldsymbol{r}_i, \dot{\boldsymbol{r}}_i\}$ to meet the requirements listed above. Detaching from the thermostat, the system then relaxes to collect the phase space trajectory under a microcanonical ensemble (NVE), from which the time-dependent $P(t)$ is estimated to obtain the value of τ following Eq. (8). Here, each relaxation case is independently repeated at least six times with different initial states to limit the statistical error.

Figure 2 plots the relaxations of $P_z(t)$, $P_x(t)$, and $P_y(t)$ at room temperature in Cases I and II, respectively. For Case I, where the system relaxes from P_0^I towards P_A, $P_z(t)$ reveals a well-defined underdamped behavior with a relaxation time of $\tau = 0.05$ ps, as shown in Fig. 2(a), while $P_x(t)$ and $P_y(t)$ show the commonly seen thermal fluctuations around their mean values of zero in Fig. 2(b). This indicates that the system basically relaxes along the ⟨001⟩ direction, and the relaxation of P_z is independent of P_x and P_y. The corresponding power spectra of $P_z(t)$, $P_x(t)$, and $P_y(t)$ during adiabatic relaxation processes of Case I are shown in Fig. 2(c). Significant differences are seen between the relaxations of $P_z(t)$, $P_x(t)$, and $P_y(t)$ in the low-frequency band. On the other hand, for Case II, the relaxation behavior of $P_x(t)$ is quite significant as shown in Fig. 2(e), with a relaxation time of $\tau = 1.17$ ps, because there is a deviation from equilibrium for the polarization along the ⟨100⟩ direction. In addition, the temporal evolution behaviors of $P_z(t)$ and $P_y(t)$ are close to those in Case I. Figure 2(f) plots the corresponding power spectra of the adiabatic relaxation processes of Case II. Note that the power spectra of $P_x(t)$ at all three frequency bands are significantly stimulated, especially the shift in the peak at the lowest frequency band, while the power spectra of $P_z(t)$ and $P_y(t)$ remain nearly unchanged. Moreover, we focus on the lowest response frequency bands of $P_x(t)$ and $P_z(t)$, ∼8 THz (see Fig. S2 in the Supplemental Material [54]), to determine the reliability of the estimation of the polarization relaxation time τ. In principle, τ corresponds to the full width at half maximum (FWHM) Γ of the spectral lines as $\tau = (2\Gamma)^{-1}$. It is found that (see Fig. S3 in the Supplemental Material [54]) $\Gamma_x \sim 1.25$ THz for $P_x(t)$ and that $\Gamma_z \sim 5.0$ THz for $P_z(t)$, respectively, therefore, $\tau_x \sim 0.4$ ps and $\tau_z = 0.10$ ps, which are comparable to the values estimated from adiabatic processes mentioned above. These results generally confirm our conclusion about polarization relaxation in the time domain. The dynamics of the polarization component at room temperature are independent of each other, and the relaxation times along the polar and nonpolar directions are quite different. As a result, the relaxation time of BTO is suggested to be a second-rank tensor with only three nonzero parameters along the principal directions.

Furthermore, the designed adiabatic processes are performed at different ferroelectric phases of BTO by varying the background temperature from 300 K to 80 K. Here, the initial

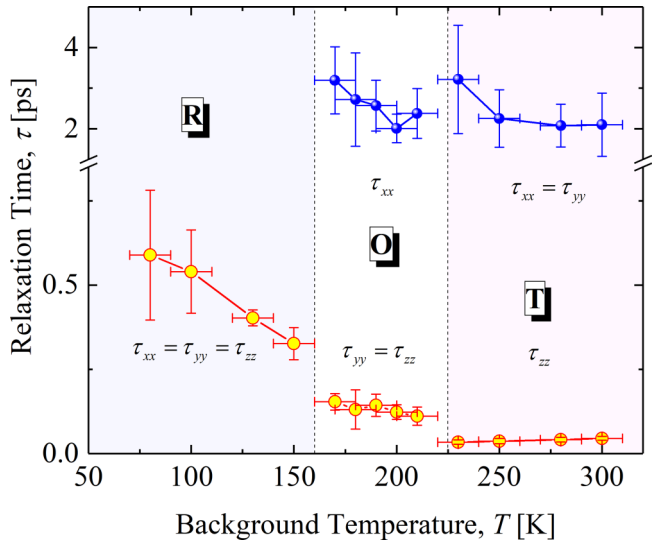

FIG. 3. Temperature dependence of the polarization relaxation time in different ferroelectric phases of $BaTiO_3$. Here, the green solid data points denote τ along the nonpolar directions without spontaneous polarization, while the red open circles represent τ along the polar directions with nonzero spontaneous polarization in a specific ferroelectric phase.

states for the adiabatic processes are set to be a small deviation Δ from the corresponding equilibrium states, similar to the settings in Cases I and II mentioned above (see details in Sec. SIV of the Supplemental Material [54]), to calculate the relaxation time of $P_x(t)$, $P_y(t)$, and $P_z(t)$. For instance, for the orthorhombic (O) phase of BTO, two cases of initial states are selected, i.e., Case I of $\boldsymbol{P}_0^{\mathrm{I}} = (0, 1+\Delta, 1+\Delta)\lambda$ and Case II of $\boldsymbol{P}_0^{\mathrm{II}} = (\Delta, 1+\Delta, 1+\Delta)\lambda$; for the rhombohedral (R) phase, because there is spontaneous polarization along the $\langle 111\rangle$ direction, only one case is considered, i.e., Case I of $\boldsymbol{P}_0^{\mathrm{I}} = (1+\Delta, 1+\Delta, 1+\Delta)\lambda$. In addition, the variance of Δ in the initial states is confirmed to have little influence on the intrinsic polarization relaxation time (see Fig. S4 in the Supplemental Material [54]). In this case, the relaxation time τ is estimated as the average value of those obtained from at least six independent MD simulations. Figure 3 plots the temperature dependence of τ in different ferroelectric phases of BTO. It is found that the τ in the nonpolar directions is approximately an order of magnitude larger than that in the polar directions, indicating much slower relaxation along the nonpolar directions. Furthermore, τ shows different temperature dependences in different ferroelectric phases. For example, $\tau_{zz} = \tau_{yy} = \tau_{xx}$ decreases with temperature from ~0.600 ps at 80 K to ~0.350 ps at 150 K in the R phase, and $\tau_{zz} = \tau_{yy}$ decreases with temperature from ~0.150 ps at 170 K to ~0.100 ps at 210 K in the O phase, while τ_{zz} shows an opposite temperature dependence from ~0.035 ps at 230 K to ~0.050 ps at 300 K in the T phase. Interestingly, for the τ in the nonpolar directions, the τ_{xx} in the O phase decreases with increasing temperature, but $\tau_{xx} = \tau_{yy}$ in the T phase does not show significant temperature dependence; however, an abrupt increasing trend occurs near the boundary of the O and T phases that is not found for τ along the polar directions, e.g., $\tau_{yy} = \tau_{zz}$ in the O phase and τ_{zz} in the T phase. This may be attributed to the slowing of the polarization relaxation due to the ferroelectric phase transition; this mechanism requires further investigation.

IV. DISCUSSION

A. Relation linking relaxation time and kinetic coefficient

As mentioned above, the GLE of Eq. (5) can be conditionally simplified to the phenomenological TDGL equation of polarization evolution on the meso- or macroscale [27,34,52]. We take the TDGL equation for example. For a ferroelectric monodomain system, the polarization evolution $P = P(t)$ follows

$$\frac{\partial P}{\partial t} = -L\frac{\partial \psi}{\partial P}, \tag{14}$$

where $\psi(P)$ is the free energy density; i.e., $F[P] = \int_V \psi(P)dV$, with $F[P]$ being the functional of P. In general, $\psi(P)$ has a symmetrical double well form when no external field is applied as

$$\psi(P) = -AP^2 + BP^4 = B(P^2 - \lambda^2)^2 - B\lambda^4. \tag{15}$$

Here, A and B are the expansion coefficients, λ is the polarization with free energy minimization, and $\lambda^2 = A/2B$. Similar to the adiabatic relaxation process designed in Sec. III, if there is a small deviation Δ in P with respect to its equilibrium state of λ, as $P = (1+\Delta)\lambda$ at $t = 0$, the increment in ψ can be approximately written as

$$\psi(P) - \psi(\lambda) \approx (P-\lambda)^2/2\chi \tag{16}$$

in the case of $\Delta \ll 1$, where χ is the dielectric constant related to the curvature of $\psi(P)$ at $P = \lambda$, and $\chi^{-1} = 8B\lambda^2$. Therefore, Eq. (14) can be simplified to

$$\dot{P} = -L\chi^{-1}(P-\lambda). \tag{17}$$

We can then obtain the evolution of $P(t)$ as

$$P(t) = \lambda(1 + \Delta e^{-Lt/\chi}). \tag{18}$$

Comparing Eq. (18) with Eq. (8), we can link the polarization relaxation time τ and kinetic coefficient through the relationship

$$L = \chi/(2\tau) = \chi/(2\langle\tau_k\rangle). \tag{19}$$

That is, the energetic dissipation rate $\gamma = \tau^{-1}$ in a ferroelectric system, written in terms of a finite lifetime of phonon modes due to phonon-phonon interactions, i.e., $\gamma = \langle\tau_k\rangle^{-1}$, is exactly the damping constant in Tani's equation [52] and is closely related to the kinetic coefficient L in the TDGL equation for the polarization evolution in a phenomenological framework.

Figure 4 plots the temperature dependence of $L = L(T)$ at different ferroelectric phases of BTO, estimated following Eq. (19), where $\tau = \tau(T)$ is obtained from Fig. 3 and $\chi = \chi(T)$ is calculated by performing MD simulations based on the fluctuation relation of polarization addressed anywhere [59] (see Sec. SVII of the Supplemental Material [54]). Referring to the estimation of τ, L is expected to be a second-rank tensor with only three nonzero parameters, i.e., L_{xx}, L_{yy}, and

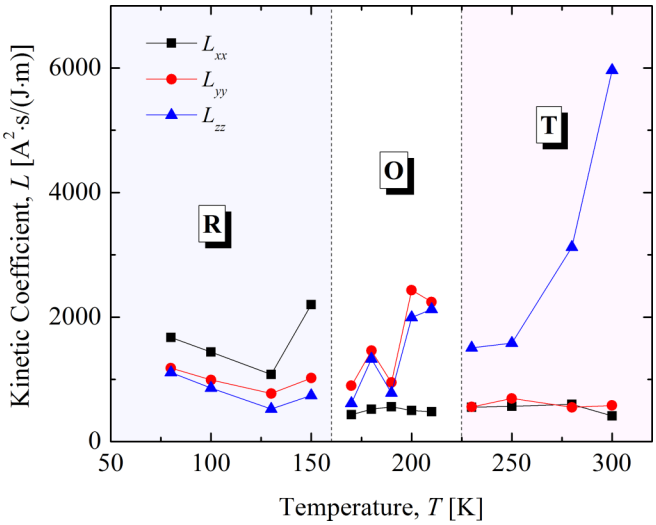

FIG. 4. The temperature dependence of the kinetic coefficient L is used to govern the polarization evolution behavior in the TDGL equation and is estimated following $L = \chi/(2\tau)$. Here, the data of $\tau = \tau(T)$ can be obtained in Fig. 3, and $\chi = \chi(T)$ is plotted in Fig. S4 in the Supplemental Material [54].

L_{zz}, where $L_{\alpha\alpha} = \chi_{\alpha\alpha}/(2\tau_{\alpha\alpha})$ with $\alpha = x, y, z$, because there is no significant coupling between the different polarization components during the relaxation process. As plotted in Fig. 4, $L_{\alpha\alpha}$ has almost the same values and temperature dependence as $L_{\beta\beta}$ (here $\beta = x, y, z$) if $P_\alpha = P_\beta$. Otherwise, there is a significant distinction between $L_{\alpha\alpha}$ and $L_{\beta\beta}$ if $P_\alpha \neq P_\beta$. In particular, $L_{\alpha\alpha}$ has a larger value in the case of $P_\alpha \neq 0$. As shown in Fig. 4, L_{xx}, L_{yy}, and L_{zz} are almost the same in the R phase because there is spontaneous polarization along the ⟨111⟩ direction. Correspondingly, L_{zz} and L_{yy} are larger than L_{xx} in the O phase, with a ⟨011⟩ spontaneous polarization, and L_{zz} is much larger than L_{xx} and L_{yy} in the T phase with spontaneous polarization along ⟨001⟩. Overall, the values of $L_{\alpha\alpha}$ are on the order of magnitude of 10^3 [A^2 s/(J m)]. In addition, the L_{zz} in the T phase exhibits a sharply increasing trend, e.g., from ∼1500 at 230 K to ∼6000 [A^2 s/(J m)] at 300 K, and L_{xx} and L_{yy} remain almost temperature independent, ∼500 [A^2 s/(J m)].

According to Eq. (19), the kinetic coefficient governing the polarization evolution in the TDGL equation is affected by both χ and τ. At first glance, because the variation of χ (see Fig. S5 in the Supplemental Material [54]) with temperature is much more dramatic than that of τ (see Fig. 3), the temperature dependence of L is mainly dominated by χ, particularly near the phase boundary. However, when L is examined from a physical point of view, χ and τ reflect different relaxation characteristics of polarization during a specific phase transition process. On one hand, the χ at various temperatures are determined to be associated with the polarization fluctuation near equilibrium (see Sec. SVII of the Supplemental Material [54]). In addition, as discussed in Sec. II, χ is related to the information of a given free energy landscape, particularly near the potential bottom of the free energy surface. Therefore, χ mainly reflects the fluctuation characteristics, which are determinant when the ferroelectric system experiences a quasiequilibrium phase transition process. On the other hand, τ reveals the dissipation nature of phase transport, which takes over when dealing with issues related to nonequilibrium phase transition processes on a given free energy surface. In our opinion, for a specific phase transition, χ mainly represents the thermodynamics of the initial and final states, while τ characterizes the dynamics during the phase transition process, both of which are represented in the kinetic coefficient used in the TDGL equation.

Moreover, the kinetic coefficient L in the TDGL equation is a key factor for the dynamical behavior of polarization in ferroelectrics. In the current work, we obtain the kinetic coefficient L as a second-rank tensor, which is different from the one used in PFM as a scalar. This is because the free energy in our model is different from that in PFM. Following Landau's theory of phase transition, the explicit expression of free energy in PFM is obtained by representing the free energy surface as a Taylor expansion of the order parameter, i.e., polarization for ferroelectrics, always taking the free energy of the cubic phase as a reference. Therefore, L in PFM reveals the symmetry of the free energy functional, i.e., in the form of a scalar, when the TDGL equation is employed in combination with the Landau free energy to simulate polarization relaxation. On the other hand, τ and the corresponding L in the current model are determined based on the free energy surface under the well-defined ferroelectric equilibrium states at the specific background temperature. That is, the L in each ferroelectric phase of BTO definitely reveals the symmetry of the crystal structure of each phase of BTO. Therefore, the L calculated in the current work should be written in the form of a second-rank tensor. The TDGL equation is a generalized phenomenological equation of motion for polarization in ferroelectrics, where various free energy functional expressions can be adopted and are not confined to the one with cubic symmetry as a reference. In fact, we are aware that there have been studies focusing on recasting the free energy used in PFM based on first-principle-derived simulations [57,60–62]. In other words, for issues about polarization relaxation in ferroelectrics, the form of L used in the TDGL equation should be determined by the expression of the free energy functional. We take a specific case of polarization relaxation inside a ferroelectric system with multidomain states as an example. If there are sufficient numbers of domains involved, which makes the whole system isotropic, PFM, with a free energy functional taking that of the cubic phase as reference and the scalar form of L, is determined to be more convenient for describing the polarization relaxation. In this scheme, the polarization relaxation along different directions is treated as identical. However, if one focuses on the dynamical behavior of polarization inside a specific domain of such a multidomain ferroelectric system, the tensor form of L is recommended to account for the anisotropic characteristics of the polarization relaxation, and the possible existing coupling or competition between the polarization along different directions. The anisotropy and possible competition between different polarization directions can be expected to have a significant influence on the polarization dynamics of the ferroelectric system, especially when the system experiences a phase transition from one ferroelectric phase to another ferroelectric phase.

In summary, based on a polarization relaxation process of a small deviation from equilibrium within a single side of double well energy landscape, i.e., from P_0 to P_A in Fig. 1(d), we discuss the physical picture of τ addressed in Eq. (19) that the polarization relaxation time τ or energy dissipation rate γ is linked to the kinetic coefficient L in phenomenological models. In the following, we apply a physical picture of τ to a case where polarization goes through the energy barrier, i.e., from P_A to P_B in Fig. 1(d), to determine the applicability and reliability of the physical picture of τ.

B. Relation linking the relaxation time and switching time

Applying a sufficiently large reversed external electric field E_{ext} on the ferroelectric domain with nonzero spontaneous polarization results in polarization switching. Considering a ferroelectric monodomain system containing N interactive local microregions with polarization P_i under an external field E_{ext}, the free energy density $\psi(P_i)$ is written as

$$\psi(P_i) = \psi_s(P_i) - \sum_j{}' (\chi^{-1} P_i P_j) - E_{\text{ext}} P_i, \tag{20}$$

where $\psi_s(P_i)$ is the self-energy in the form of a symmetrical double well, the second term in *rhs* is the interaction between P_i and its neighbors P_j, and the term $-E_{\text{ext}}P_i$ denotes the effect of the external electric field applied. In the case of $|E_{\text{ext}}| > E_{\text{crit}}$($E_{\text{crit}}$ is the thermodynamic coercive field [34]), the polarization undergoes a fast switching process, analogous to the driven Brownian motion, where the energy barrier related to $\psi_s(P_i)$ has little influence [34,41]. In addition, the actions of the neighboring P_j in Eq. (20) provide an internal field $E_{\text{int}} = \sum_j{}' \chi^{-1} P_j$ governing the motion of P_i, which can then be written as

$$E_{\text{int}} = \sum_j{}' \chi^{-1} P_j \approx \sum_j{}' \chi^{-1} \langle P_j \rangle = \chi^{-1} P \tag{21}$$

under the mean-field approximation. Here, P is the total polarization as the ensemble average over all the microregions involved, and $P = \langle P_j \rangle$. In this regard, in the case of $|E_{\text{ext}}| > E_{\text{crit}}$,

$$\psi(P_i) \approx -(E_{\text{int}} + E_{\text{ext}}) P_i. \tag{22}$$

Following the TDGL equation of Eq. (14), we have the evolution equation as

$$\dot{P} = L(\chi^{-1} P + E_{\text{ext}}), \tag{23}$$

where the evolution rate of the total polarization $\dot{P}$ is equivalent to $\langle \dot{P}_i \rangle$ under the assumption that $\partial \langle P_i \rangle / \partial t = \langle \partial P_i / \partial t \rangle$ in a ferroelectric monodomain state.

We consider a polarization switching process, where the polarization $P = \lambda$ is switching to $P = -\lambda$ by an external field $E_{\text{ext}} = -E$. The switching time t_s is defined as the time interval for $P = P(t)$ switching from λ to zero, as

$$\int_0^{t_s} dt = \int_\lambda^0 \frac{dP}{L(\chi^{-1} P - E)}. \tag{24}$$

Solving Eq. (24), we have

$$t_s = -2\tau \ln[1 - E_{\text{crit}}/E] \quad \text{or} \quad e^{-t_s/2\tau} = 1 - E_{\text{crit}}/E. \tag{25}$$

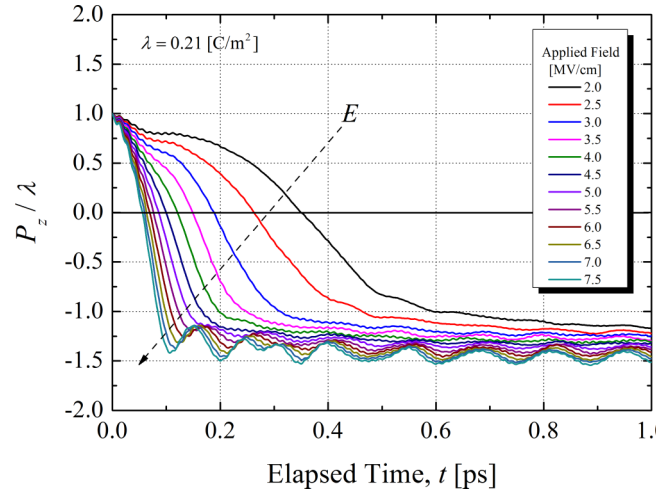

FIG. 5. The polarization switching processes of $BaTiO_3$ at 300 K under various applied reversal external electric fields $E_{\text{ext}} = -E$ ranging from 2.0 to 7.5 MV/cm.

Here, $\tau = \chi/(2L)$ is actually the polarization relaxation time discussed in the foregoing section. The thermodynamic coercive field $E_{\text{crit}} = \lambda/\chi$ can be estimated from the ferroelectric hysteresis loop, e.g., $E_{\text{crit}} = 2.6$ (MV/cm) of BTO at 300 K (see Fig. S6 in the Supplemental Material [54]).

Figure 5 demonstrates the switching processes in the T phase of BTO under various $E_{\text{ext}} = -E$ with strengths of E ranging from 2.0 to 7.5 (MV/cm) by performing MD simulations at room temperature. Before E_{ext} is applied, 10 ps of MD runs with a time step of 0.4fs and a canonical ensemble are carried out to obtain the equilibrium state of the monodomain with a spontaneous polarization of $P_z = \lambda$ at $t = 0$. Subsequently, a constant reversed $E_{\text{ext}} = -E$ is applied to drag the polarization in the opposite direction. Plotted in Fig. 5, t_s is found to sensitively decrease as the strength of E_{ext} increases, e.g., from $t_s = 0.35$ ps for $E = 2.5$ (MV/cm) to $t_s = 0.05$ ps for $E = 7.5$ (MV/cm), which is much faster than that under a small applied field, with several (MV/m) reported [34]. Figure 6(a) plots the relation of t_s and E written in the form of $e^{-t_s/2\tau} = 1 - E_{\text{crit}}/E$, with a comparison between the dynamical simulation data of t_s and the theoretical predictions in Eq. (25), where $E_{\text{crit}} = 2.6$ (MV/cm) is estimated from the ferroelectric hysteresis loop (see Fig. S6 in the Supplemental Material [54]) and $\tau = 0.05$ ps as shown in Fig. 3. Good consistency can be found when $E > E_{\text{crit}}$, which confirms the applicability and reliability of the physical picture of the polarization relaxation time τ clarified in the current paper. On the other hand, we fit the simulation data following Merz's Law; i.e., $t_s^{-1} = \tau^{-1} e^{-E_{\text{crit}}/E}$. As shown in Fig. 6(b), Merz's law can also describe the E dependence of t_s well, especially when $E \geqslant 3$ (MV/cm). However, the $\tau = 0.018$ ps and $E_{\text{crit}} = 6.65$ (MV/cm) obtained as fitting parameters using Merz's law significantly deviate from the MD simulation estimations. Moreover, Merz's law should be applicable in the case of small applied field strength, which conflicts with the results in Fig. 6(b) and similar switching behaviors in ferroelectric nanowires reported in Ref. [63].

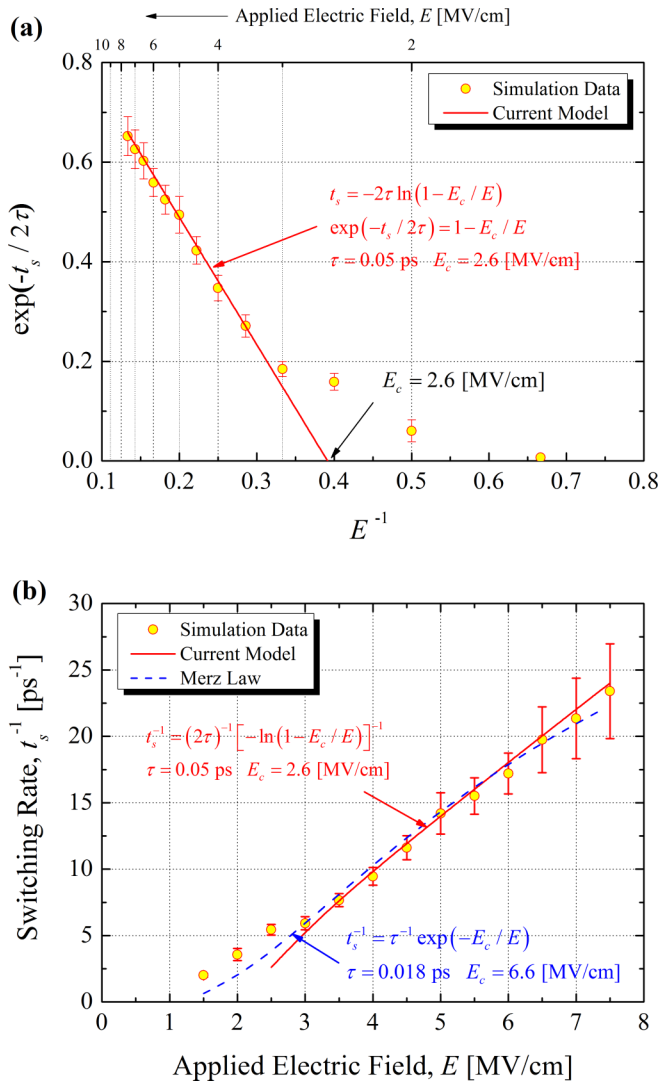

FIG. 6. The dependence of the polarization switching time t_s on the applied external electric field E. The "Simulation data" represent the results estimated from the switching processes t_s shown in Fig. 5 and are compared to (a) the prediction (denoted the "Current Model," with a red solid line) of our model derived based on the physical picture of relaxation time τ introduced in generalized Langevin equation of Eq. (5), i.e., $e^{-t_s/2\tau} = 1 - E_{\rm crit}/E$. Here, $\tau = 0.05$ ps is illustrated in Fig. 2, and $E_{\rm crit} \sim 2.6$ MV/cm is the thermodynamic coercive field estimated by the ferroelectric hysteresis loop shown in Fig. S5 in the Supplemental Material [54]. (b) The corresponding switching rate t_s^{-1} as a function of E and the comparison of the dynamical simulation data with theoretical predictions following the current model and Merz's law [37], i.e., $t_s^{-1} = \tau^{-1} e^{-E_{\rm crit}/E}$. A detailed discussion can be found in context.

Note that the theoretical model of Eq. (25) is derived based on the assumption that micropolar regions are unit-cell dipoles involved in a ferroelectric monodomain system, whose switching corresponds to the directional rotation along the energetic optimal path upon their "potential" landscape. In fact, as addressed in Ref. [64], more complicated many-body effects are responsible for dipole flip-flop motion during the relaxation process, but these effects are not considered in the current model. Furthermore, Eq. (25) is appropriated in the limit of $E > E_{\rm crit}$ because of the logarithm function in Eq. (25). Therefore, further investigation is required to expand our model to the case of $E < E_{\rm crit}$, as illustrated in Fig. 5, where ultrafast polarization switching can be observed in many-body dynamical simulations.

V. CONCLUSION

In this paper, on the basis of atomic simulations, we discussed the temporal characteristics of polarization relaxation in ferroelectric materials by taking $BaTiO_3$ as an example. Starting from a many-body ferroelectric system involving weakly interactive phonon modes, we proposed a generalized Langevin equation with a form similar to that of the evolution equation in a recently developed dynamical phase field model to describe the dynamical evolution of the observed polarization on the meso- or macroscale. An adiabatic process was artificially designed, and a simple relation between the polarization relaxation time and the lifetime of the phonon modes in a many-body system was derived to bridge the meso- or macroscale modeling scheme with the corresponding microscale dynamics. Although the validity of this relation was not directly verified in the current paper, we designed two application scenarios to discuss the applicability and reliability of the physical picture of the polarization relaxation time. First, from the designed adiabatic relaxation process of polarization, we calculated the temperature dependence of the relaxation time, which was linked to the kinetic coefficient describing the polarization evolution feature in the phenomenological model, such as the time-dependent Ginzburg-Landau equation used in the phase field model. Second, we proposed a formula describing the dependence of the polarization switching time on the applied external electric field. The good consistency between the theoretical prediction and simulation data confirmed the applicability and reliability of the physical picture of the relaxation time. Although the theoretical models and atomic simulations in the current report are restricted to a simple case, i.e., a ferroelectric monodomain system, and must be carefully examined when expanded to a complicated system, the discussion of the physical picture of the relaxation time could provide useful ideas for the development of a multiscale modeling scheme for ferroelectrics.

ACKNOWLEDGMENTS

This work was supported by the National Natural Science Foundation of China (NSFC) Grants No. 11972382 and No. 12002400, and the Guangzhou Science and Technology Projects No. 201707020002 and No. 2019060001.

[1] T. Qi, Y.-H. Shin, K.-L. Yeh, K. A. Nelson, and A. M. Rappe, Phys. Rev. Lett. **102**, 247603 (2009).

[2] R. Mankowsky, A. von Hoegen, M. Först, and A. Cavalleri, Phys. Rev. Lett. **118**, 197601 (2017).

[3] Z. Gu, S. Pandya, A. Samanta, S. Liu, G. Xiao, C. J. Meyers, A. R. Damodaran, H. Barak, A. Dasgupta, S. Saremi, A. Polemi, L. Wu, A. A. Podpirka, A. Will-Cole, C. J. Hawley, P. K. Davies, R. A. York, I. Grinberg, L. W. Martin, and J. E. Spanier, Nature (London) **560**, 622 (2018).

[4] J. Liu, Y. Ji, S. Yuan, L. Ding, W. Chen, and Y. Zheng, npj Comput. Mater. **4**, 78 (2018).

[5] C. Paillard, E. Torun, L. Wirtz, J. Íñiguez, and L. Bellaiche, Phys. Rev. Lett. **123**, 087601 (2019).

[6] R. Blinc and B. Žekš, in *Soft Modes in Ferroelectrics and Antiferroelectrics* (North-Holland, Amsterdam, 1974), Chap. 2, pp. 50–56.

[7] J. Li, B. Nagaraj, H. Liang, W. Cao, C. H. Lee, and R. Ramesh, Appl. Phys. Lett. **84**, 1174 (2004).

[8] A. Grigoriev, D.-H. Do, D. M. Kim, C.-B. Eom, B. Adams, E. M. Dufresne, and P. G. Evans, Phys. Rev. Lett. **96**, 187601 (2006).

[9] A. Gruverman, D. Wu, and J. F. Scott, Phys. Rev. Lett. **100**, 097601 (2008).

[10] N. A. Pertsev, A. Petraru, H. Kohlstedt, R. Waser, I. K. Bdikin, D. Kiselev, and A. L. Kholkin, Nanotechnology **19**, 375703 (2008).

[11] D. Zhao, I. Katsouras, K. Asadi, P. W. M. Blom, and D. M. de Leeuw, Phys. Rev. B **92**, 214115 (2015).

[12] Q. Meng, M.-G. Han, J. Tao, G. Xu, D. O. Welch, and Y. Zhu, Phys. Rev. B **91**, 054104 (2015).

[13] D. Wang, A. A. Bokov, Z. G. Ye, J. Hlinka, and L. Bellaiche, Nat. Commun. **7**, 11014 (2016).

[14] F. Chen, Y. Zhu, S. Liu, Y. Qi, H. Y. Hwang, N. C. Brandt, J. Lu, F. Quirin, H. Enquist, P. Zalden, T. Hu, J. Goodfellow, M.-J. Sher, M. C. Hoffmann, D. Zhu, H. Lemke, J. Glownia, M. Chollet, A. R. Damodaran, J. Park, Z. Cai, I. W. Jung, M. J. Highland, D. A. Walko, J. W. Freeland, P. G. Evans, A. Vailionis, J. Larsson, K. A. Nelson, A. M. Rappe, K. Sokolowski-Tinten, L. W. Martin, H. Wen, and A. M. Lindenberg, Phys. Rev. B **94**, 180104(R) (2016).

[15] S. Gorfman, A. A. Bokov, A. Davtyan, M. Reiser, Y. Xie, Z. G. Ye, A. V. Zozulya, M. Sprung, U. Pietsch, and C. Gutt, Proc. Natl. Acad. Sci. USA **115**, E6680 (2018).

[16] C. Elissalde and J. Ravez, J. Mater. Chem. **11**, 1957 (2001).

[17] J. Y. Jo, S. M. Yang, T. H. Kim, H. N. Lee, J.-G. Yoon, S. Park, Y. Jo, M. H. Jung, and T. W. Noh, Phys. Rev. Lett. **102**, 045701 (2009).

[18] C. M. Fancher, S. Brewer, C. C. Chung, S. Röhrig, T. Rojac, G. Esteves, M. Deluca, N. Bassiri-Gharb, and J. L. Jones, Acta Mater. **126**, 36 (2017).

[19] M. Sepliarsky, S. R. Phillpot, S. K. Streiffer, M. G. Stachiotti, and R. L. Migoni, Appl. Phys. Lett. **79**, 4417 (2001).

[20] Y. H. Shin, I. Grinberg, I. W. Chen, and A. M. Rappe, Nature (London) **449**, 881 (2007).

[21] I. Grinberg, Y.-H. Shin, and A. M. Rappe, Phys. Rev. Lett. **103**, 197601 (2009).

[22] S. Liu, I. Grinberg, and A. M. Rappe, Nature (London) **534**, 360 (2016).

[23] V. Boddu, F. Endres, and P. Steinmann, Sci. Rep. **7**, 806 (2017).

[24] T. Nishimatsu, U. V. Waghmare, Y. Kawazoe, and D. Vanderbilt, Phys. Rev. B **78**, 104104 (2008).

[25] S. Lisenkov, I. Ponomareva, and L. Bellaiche, Phys. Rev. B **79**, 024101 (2009).

[26] Q. Zhang, R. Herchig, and I. Ponomareva, Phys. Rev. Lett. **107**, 177601 (2011).

[27] H. Akamatsu, Y. Yuan, V. A. Stoica, G. Stone, T. Yang, Z. Hong, S. Lei, Y. Zhu, R. C. Haislmaier, J. W. Freeland, L.-Q. Chen, H. Wen, and V. Gopalan, Phys. Rev. Lett. **120**, 096101 (2018).

[28] T. Yang, B. Wang, J.-M. Hu, and L.-Q. Chen, Phys. Rev. Lett. **124**, 107601 (2020).

[29] S. R. Phillpot, S. B. Sinnott, and A. Asthagiri, Annu. Rev. Mater. Res. **37**, 239 (2007).

[30] A. Kumar and U. V. Waghmare, Phys. Rev. B **82**, 054117 (2010).

[31] D. Fang, F. Li, B. Liu, Y. Zhang, J. Hong, and X. Guo, Appl. Mech. Rev. **65**, 060802 (2013).

[32] J. Liu, W. Chen, B. Wang, and Y. Zheng, Materials **7**, 6502 (2014).

[33] L. Li, Y. Cao, S. Somnath, Y. Yang, S. Jesse, Y. Ehara, H. Funakubo, L. Q. Chen, S. V. Kalinin, and R. K. Vasudevan, Adv. Electron. Mater. **3**, 1600508 (2017).

[34] A. K. Tagantsev, L. E. Cross, and J. Fousek, in *Domains in Ferroic Crystals and Thin Films* (Springer, New York, 2010), Chap. 8, pp. 448–483.

[35] B. Caroli, C. Caroli, and B. Roulet, J. Stat. Phys. **21**, 415 (1979).

[36] S. Boyn, J. Grollier, G. Lecerf, B. Xu, N. Locatelli, S. Fusil, S. Girod, C. Carrétéro, K. Garcia, S. Xavier, J. Tomas, L. Bellaiche, M. Bibes, A. Barthélémy, S. Saïghi, and V. Garcia, Nat. Commun. **8**, 14736 (2017).

[37] W. J. Merz, Phys. Rev. **95**, 690 (1954).

[38] G. Henkelman, Phys. Rev. B **102**, 035308 (2020).

[39] T. D. Swinburne, S. L. Dudarev, S. P. Fitzgerald, M. R. Gilbert, and A. P. Sutton, Phys. Rev. B **87**, 064108 (2013).

[40] T. D. Swinburne, S. L. Dudarev, and A. P. Sutton, Phys. Rev. Lett. **113**, 215501 (2014).

[41] H. Wen, A. Semenov, and C. Woo, J. Nucl. Mater. **493**, 21 (2017).

[42] K. Lai, H. Wen, J. Liu, Y. Wu, and Y. Zheng, J. Nucl. Mater. **524**, 286 (2019).

[43] G. Vizdrik, S. Ducharme, V. M. Fridkin, and S. G. Yudin, Phys. Rev. B **68**, 094113 (2003).

[44] M. J. Highland, T. T. Fister, M.-I. Richard, D. D. Fong, P. H. Fuoss, C. Thompson, J. A. Eastman, S. K. Streiffer, and G. B. Stephenson, Phys. Rev. Lett. **105**, 167601 (2010).

[45] R. Gaynutdinov, S. Yudin, S. Ducharme, and V. Fridkin, J. Phys.: Condens. Matter **24**, 015902 (2011).

[46] R. V. Gaynutdinov, S. Mitko, S. G. Yudin, V. M. Fridkin, and S. Ducharme, Appl. Phys. Lett. **99**, 142904 (2011).

[47] J. M. Vielma and G. Schneider, J. Appl. Phys. **114**, 174108 (2013).

[48] M. Born and K. Huang, *Dynamical Theory of Crystal Lattices* (Clarendon Press, Geoffrey Cumberlege, Oxford, 1954).

[49] R. Zwanzig, J. Chem. Phys. **33**, 1338 (1960).

[50] H. Mori, Prog. Theor. Phys. **34**, 399 (1965).

[51] G. Geneste, L. Bellaiche, and J.-M. Kiat, Phys. Rev. Lett. **116**, 247601 (2016).

[52] K. Tani, Phys. Lett. A **25**, 400 (1967); J. Phys. Soc. Jpn. **26**, 93 (1969).

[53] L. D. Landau and I. M. Khalatnikov, Dokl. Akad. Nauk SSSR **96**, 469 (1954).

[54] See Supplemental Material at http://link.aps.org/supplemental/10.1103/PhysRevB.103.014308 for deduction of microdynamic expression of relaxation time (Section SI), calculation of the

free energy at room temperature (Sec. SII), design of adiabatic relaxation process (Sec. SIV), discussion about statistical error in the estimation of τ (Sec. SVI), and simulated phase diagram (Sec. SIII), power spectra of $P(t)$ (Sec. SV), dielectric constant (Sec. SVII) and hysteresis loop (Sec. SVIII) of $BaTiO_3$.

[55] S. Tinte, M. G. Stachiotti, M. Sepliarsky, R. L. Migoni, and C. O. Rodriguez, J. Phys.: Condens. Matter **11**, 9679 (1999).

[56] W. Zhong, D. Vanderbilt, and K. M. Rabe, Phys. Rev. B **52**, 6301 (1995).

[57] G. Geneste, Phys. Rev. B **79**, 064101 (2009).

[58] J. Y. Liu, W. J. Chen, B. Wang, and Y. Zheng, J. Appl. Phys. **114**, 044101 (2013).

[59] T. Hashimoto and H. Moriwake, Mol. Simul. **41**, 1074 (2015).

[60] B. Völker, P. Marton, C. Elsässer, and M. Kamlah, Continuum Mech. Thermodyn. **23**, 435 (2011).

[61] B. Völker, C. M. Landis, and M. Kamlah, Smart Mater. Struct. **21**, 035025 (2012).

[62] R. Indergand, A. Vidyasagar, N. Nadkarni, and D. M. Kochmann, J. Mech. Phys. Solids **144**, 104098 (2020).

[63] K. McCash, A. Srikanth, and I. Ponomareva, Phys. Rev. B **86**, 214108 (2012).

[64] A. K. Jonscher, L. A. Dissado, and R. M. Hill, Phys. Stat. Solidi (b) **102**, 351 (1980); A. K. Jonscher, J. Mater. Sci. **16**, 2037 (1981).